Article ID: 1000-324X(2020)04-0497-08 **DOI:** 10.15541/jim20190133

SnS_2 Nanoplates: Synthesis and NO_2 Sensing Property

SHAN Wei[1,2], FU Zhengqian[1], ZHANG Faqiang[1], MA Mingsheng[1], LIU Zhifu[1,2], LI Yongxiang[1,2]

(1. Shanghai Institute of Ceramics, Chinese Academy of Sciences, Shanghai 200050, China; 2. Center of Materials Science and Optoelectronics Engineering, University of Chinese Academy of Sciences, Beijing 100049, China)

Abstract: Two-dimensional (2D) metal sulfide materials are ideal for use in gas sensing applications due to their low electronic noise and a large specific surface area, and the research on highly efficient and morphologically controllable methods for preparing two-dimensional metal sulfide materials is necessary. Highly crystalline 2D hexagonal SnS_2 nanoplates (NPs) with different morphologies were prepared by high temperature chemical bath method. SnS_2 NPs were characterized by different techniques, and their gas sensing properties were further investigated. The results show that when the molar ratio of oleic acid (OAc) to oleylamine (OAm) is 1∶1, the shape of typical SnS_2 NPs is a uniform hexagon, with a diameter of about 150 nm and a thickness of 4−6 nm. The gas sensing test shows typical SnS_2 NPs are responsive to NO_2 gas, and the sensing process is reversible and selective. The optimal operating temperature is 130 ℃, and the response and recovery time are 98 and 680 s, respectively.

Key words: NO_2 gas; 2D materials; SnS_2; chemical bath synthesis; gas sensing detection

With the development of society, the detection of various gases is becoming more and more important in industrial production and environmental protection[1-2]. At present, semiconductor gas sensors based on oxide gas sensing materials are most widely used due to their high sensitivity, ease of fabrication, simple structure and low cost[3]. For example, WO_3, ZnO, and SnO_2 are used to make ethanol, acetone, and nitrogen dioxide sensors, respectively[4-6]. However, most oxide semiconductor gas sensors tend to exhibit high operating temperatures, poor sensing selectivity and high limits of detection (LODs)[7-9].

In recent years, two-dimensional (2D) transition metal dichalcogenides (TMDs) became a research hotspot in the field of nanomaterials[10-11]. TMDs are promising gas sensing materials due to their planar crystal structure, large surface-to-volume ratio and low electronic noise[12-13], which have not received deserved attention. Perkins, *et al*[14] prepared a gas sensor using MoS_2 single-layer nanosheets obtained by the Scotch tape method. It was found that the gas sensor based on this MoS_2 single-layer nanosheet had a fast response to triethylamine and acetone. The response time of triethylamine gas is less than 15 s, and this sensor can detect triethylamine gas at concentrations as low as 10^{-8}. Studies by Perkins, *et al*[14] have also shown that MoS_2-based sensors have better selectivity than carbon nanotube sensors. In particular, this MoS_2 nanosheet sensor has not strength response to water vapor, which is very important for the practical application of the sensor. Li, *et al*[15] found that Metal-Oxide-Semiconductor Field-Effect Transistors (MOSFETs) based on MoS_2 nanosheets prepared by mechanical stripping can detect NO gas at concentrations as low as 0.8×10^{-6}. The synthesis of TMDs nanoplates (NPs) with controlled size has been of scientific and technological interest. Although tin is not belong to transition metal, SnS_2 shares the similar layered structure with the TMDs. SnS_2 has a layered hexagonal structure (a=0.3645 nm, c=0.5891 nm, space group: P3m1). It is composed of tin atoms sandwiched between two layers of hexagonally disposed close packed sulfur atoms, the adjacent sulfur layers are connected by the weak van der Waals bonding. Bulk SnS_2 is a semiconductor with a band gap of 2.35 eV[16], which offers interesting applications in the fields of gas sensing. In the past few years, a few preparation methods have been developed for preparing ultrathin SnS_2 NPs. Huang, *et al*[17] reported a FET based on monolayer SnS_2 flake by exfoliating SnS_2 crystals and explored its potential application in photodetection. Su, *et al*[18] obtained the thin crystal arrays of SnS_2 at predefined locations, introducing a new idea for large-scale production by chemical vapor deposition. Unfortunately,

Received date: 2019-3-29; **Revised date:** 2019-06-25
Foundation item: National Natural Science Foundation of China (51502325, 61601444)
Biography: SHAN Wei(1989–), male, PhD candidate. E-mail: 258897449@qq.com
山 巍(1989–), 男, 博士研究生. E-mail: 258897449@qq.com
Corresponding author: LI Yongxiang, professor. E-mail: yxli@mail.sic.ac.cn; LIU Zhifu, professor. E-mail: liuzf@mail.sic.ac.cn
李永祥, 研究员. E-mail: yxli@mail.sic.ac.cn; 刘志甫, 研究员. E-mail: liuzf@mail.sic.ac.cn

due to obstacles such as high cost, difficulty of control, small output, the exfoliating and CVD methods are difficult to be used for large-scale production. Therefore, a facile, inexpensive and productive synthesis approach for SnS_2 NPs with good morphology and reduced thickness is still an important step to explore its future actual application. So simply synthesis route of wet chemistry method have attracted the attention of researchers.

However, the raw materials used in the reported hydrothermal approaches, especially the organometallic precursors and sulphureous sources (*e.g.* carbon disulfide, thioacetamide, thiourea), are toxic and expensive, thus limiting their practical applications[16,19-20]. Recently, Kumar, *et al*[21] prepared SnS_2 hexagonal nanoplates (NPs) by hydrothermal synthesis, with $SnCl_4·5H_2O$ and sulfur used as precursors, which are cheap and environmental friendly. But the lateral size of these SnS_2 NPs is less than 60 nm, and the standard diameter of 2D materials is 100 nm[22]. In addition, Du, *et al*[23] demonstrated a one-pot chemical solution-phase approach to synthesize SnS_2 nanoplates using $SnCl_4·5H_2O$ and sulfur powder as precursors. The size of samples is uniform, but their thickness is (35±10) nm, which may mask some unique properties of few-layer-structure SnS_2 NPs.

In this work, we report a facile chemical bath method to synthesize uniform 2D SnS_2 NPs in the presence of oleylamine (OAm), and oleic acid (OAc). The gas sensing results of the typical 2D SnS_2 NPs show a high response, selectivity, as well as low operating temperatures toward NO_2.

1 Experimental

1.1 Reagents

Tin (IV) chloride ($SnCl_4·5H_2O$, >99.9%, Aladdin) and sulfur powder (99.999%, Aladdin) were used as tin and sulfide precursor, respectively; oleic acid (OAc, >90.0%, Aladdin) and oleylamine (OAm, >90.0%, Aladdin), were used as surfactant; octadecene (ODe, >90.0%, Aladdin) was solvent. All the chemical reagents were used as received without further purification.

1.2 Materials preparation

Fig. 1 is an experimental steps diagram. A simplified Schlenk line was used to protect the reaction from oxygen and moisture, and the whole synthesis process should be under a persistent flow of high-purity N_2. In a typical experiment, $SnCl_4·5H_2O$ (1 mmol) was added to a mixture of OAc (10 mL) and ODe (20 mL) in a 100 mL three-neck flask. The mixed solution was degassed at 130 ℃ for 0.5 h to remove the moisture and the oxygen. Subsequently, the solution was heated to 280 ℃ within 15 min with a vigorous stir (700 r/min). The OAm-S

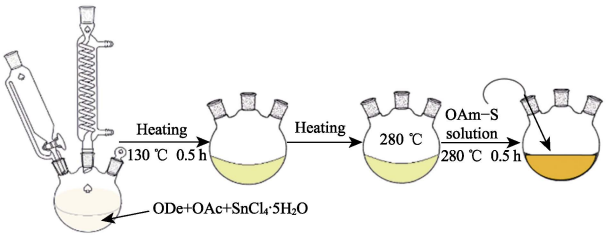

Fig. 1 Diagram of chemical bath synthesis process of 2D SnS_2 NPs

solution (sulfide powder 2 mmol was dispersed into OAm 10 mL) was injected into the reaction system and the reaction was maintained at 280 ℃ for 30 min. After cooling the solution to room temperature naturally, the yellow-green product was collected and separated from the solution by centrifugation. The product was further washed twice by ethanol and cyclohexane (1/1, *V*/*V*) and finally dispersed in cyclohexane. Besides, different morphologies of products were checked by various amount of OAm/OAc while keep other parameters unchanged. The products are stable in air without further protection for further characterizations.

1.3 Characterization

The shape and phase of the resulting SnS_2 NPs were examined by scanning electron microscopy (SEM) JEOL S4800 equipped with an energy-dispersive X-ray spectroscope (EDS) and transmission electron microscope (TEM) using a JEM-2100F (JEOL) at an accelerating voltage of 200 kV. Powder X-ray diffraction (XRD) patterns were taken on χ'Pert Pro MPD (Philips PANanalytical) with Cu-Kα radiation at 45 kV and 40 mA. The XRD data was collected with the θ-2θ scanning scope started from 2θ=10º to 80º with a step of 6 (°)/s by using Cu-Kα radiation (0.15418 nm). The composition of the reaction liquid is characterized by Fourier Transform Infrared spectrometer (FT-IR, 8400 Shimadzu, Japan).

1.4 Gas sensing performance test

To make the gas sensing device, 0.1 g of as-prepared typical SnS_2 NPs and 5 mL of cyclohexane were added into a centrifuge tube with 5 mL capacity. This mixture was ultrasonicated for 10 min to form a concentrated suspension. There are two gold signal electrodes on the front of the flat gas sensing device (shown in Fig. 2(a)) with a platinum wire connecting to each electrode. The SnS_2-cyclohexane solution was dropped on the front surface of the device and then dried in ambient air naturally. Repeating the above processes 10 times, a gas sensing tablet whose front surface was completely and evenly covered by SnS_2 NPs was prepared. On the back of the device there is heating coating of rhodium, and the operating temperature of the gas sensor is controlled by the voltage across the heating coating.

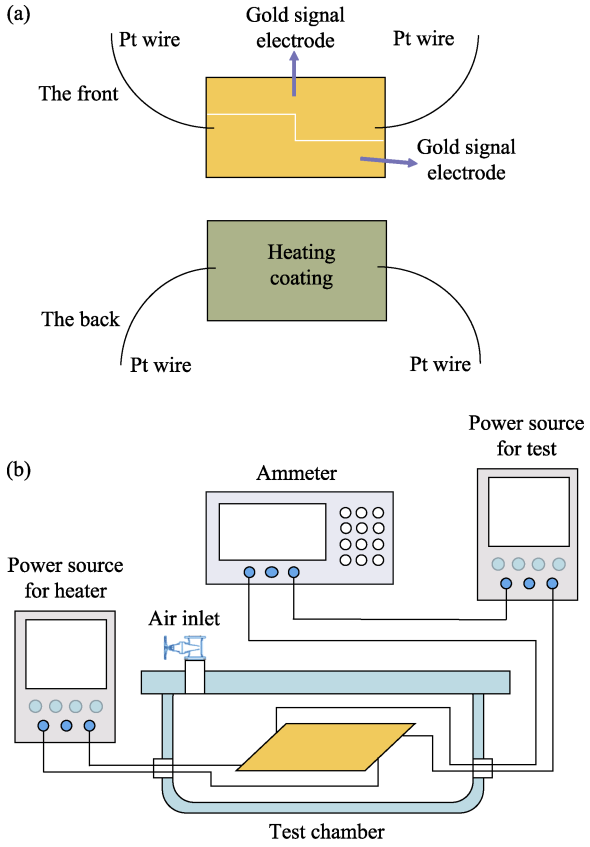

Fig. 2　(a) Schematic diagram of the device for gas sensing testing, and (b) circuit diagram of gas sensing test system

Gas sensing tests were carried out on a self-built measurement system (shown in Fig. 2(b)) using ambient air as the dilute and reference gas. The operating temperature is controlled by the heating voltage applied to the back of the test device. A hygrometer showed a humidity of 60% at room temperature (25 ℃). The sensing time (t_{sen}) or recovery time (t_{rec}) is expressed as the time for the sensor output reaching 90% of its saturation after the test gas is applied or deactivated in a function step. The response S was defined as:

$$S = R_g / R_a \tag{1}$$

where R_a and R_g are the steady-state resistances in air and gas.

2　Results and discussion

2.1　Phase analysis

XRD analysis was applied to identify the crystal structure of typical SnS_2 NPs. Fig. 3(a) shows the powder XRD pattern of as-prepared SnS_2 NPs. All the diffraction peaks and relative intensity of samples are in accord with those of bulk SnS_2 and can be indexed as the 2H hexagonal structure, which is consistent with the standard data file (ICDD 23-0677). The 2H SnS_2 belongs to the space group (P-3m1) and has three atoms in the unit cell, which extend over only one monolayer. As described in

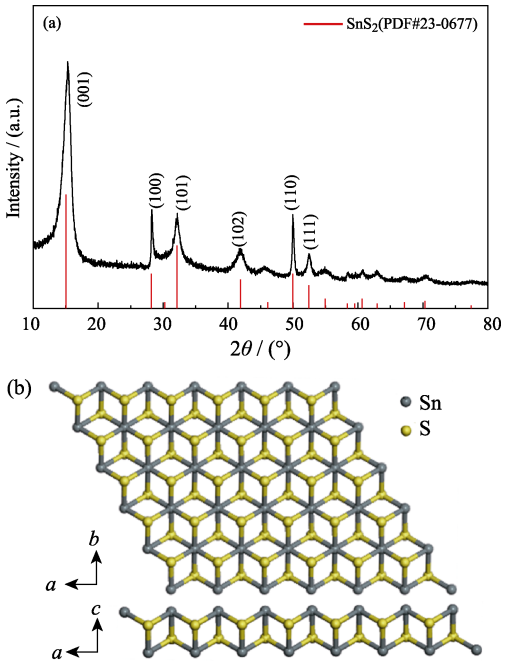

Fig. 3　(a) XRD pattern of typical SnS_2 NPs, and (b) top and cross-sectional schematics of monolayer SnS_2

Fig. 3(b), in this SnS_2 crystal, each Sn atom is six-fold coordinated, hexagonally packed between two three-fold coordinated S atoms, and S-Sn-S quintuple-layers are weakly bonded to other layers by van der Waals force. The primary diffraction peaks of as-prepared SnS_2 NPs at 2θ=15.04°, 28.27°, 32.17°, 41.95°, 50.05°, and 52.41° are respectively ascribed to the (001), (100), (101), (102), (110) and (111) planes, which is in accordance with pure 2H SnS_2 phase.

2.2　Morphology analysis

The obtained typical 2D nanoplates demonstrate unified hexagonal shape with lateral dimensions mainly ranging from 120 to 160 nm according to the SEM and TEM images shown in Fig. 4(a, b), respectively. As shown in Fig. 4(c), the cross-sectional high-resolution TEM (HRTEM) image of 2D SnS_2 flakes and its inset statistics obviously describe their layer structure and confirms that these 2D SnS_2 flakes consist of an average of (9±2) layers with an interlayer distance of 0.59 nm (profile intensity image along the line in Fig. 4(c). Fig. 4(d) shows the HRTEM image of the region circled by yellow rectangle in Fig. 4(c), in which a lattice fringe spacing of 0.318 nm is identified and corresponds to both the $(\bar{1}100)$ and $(01\bar{1}0)$ lattice planes of hexagonal SnS_2, while 0.587 nm is the distance between two adjacent (0001) molecular layers. To further confirm the growth crystalline of SnS_2 NPs, we performed EDS spectrum for the sample shown in Fig. 4(e). As shown in it, strong signals from Sn (L) and S (K) were detected by EDS. The peaks related to Al, O, C came from the Al_2O_3

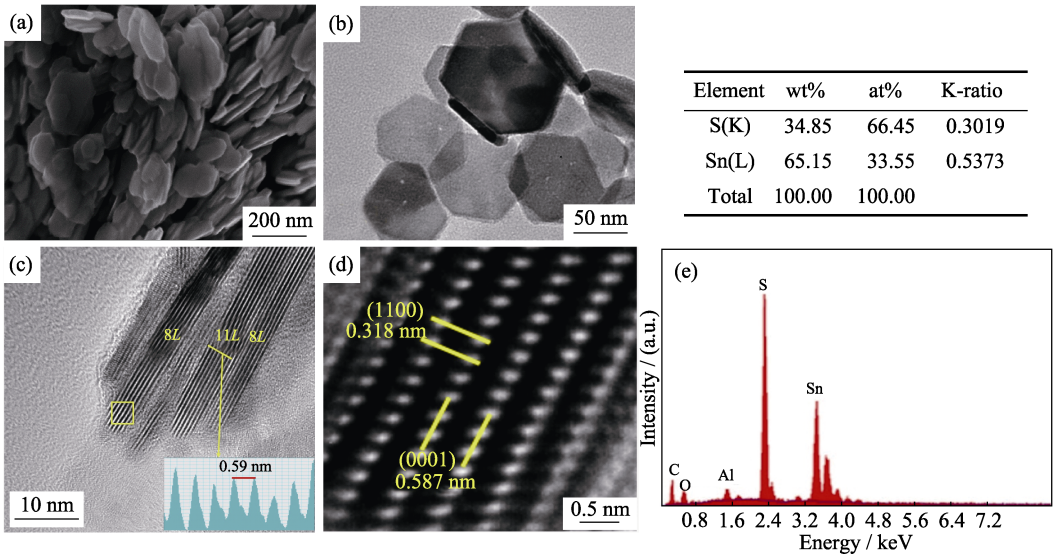

Element	wt%	at%	K-ratio
S(K)	34.85	66.45	0.3019
Sn(L)	65.15	33.55	0.5373
Total	100.00	100.00	

Fig. 4 (a) SEM image of 2D SnS_2 NPs, (b) TEM image of 2D SnS_2 NPs, (c) cross-sectional HRTEM of 2D SnS_2 NPs, (d) zoomed-in HRTEM image, and (e) EDS spectrum of 2D SnS_2 NPs

substrate used in the SEM analysis. The estimated composition was 1 : 2, exactly showing the theoretical value of SnS_2. Combined with the observed hexagonal structure and lattice images, the NPs grown by our method are concluded to be single-crystalline SnS_2.

2.3 Reaction principle and morphology control

Here, we discuss the reaction course of SnS_2 NPs formation in current approach. In the process of heating at 130 ℃, $SnCl_4{\cdot}5H_2O$ was dissolved in ODe with the help of oleic acid. It is supposed to be a replacement reaction between $SnCl_4$ and oleic acid at high temperature showing in the following reaction equation:

$$SnCl_4 + R-COOH \Rightarrow (R-COO)_4\,Sn + HCl\uparrow \qquad (2)$$

We passed the effluent gas through a flask with deionized water, and after reaction the water became acidic. This proves the formation of hydrochloric acid.

After completion of the reaction, the suspension was allowed to stand for 6 h with 5 mL of ethanol, and the FT-IR spectrum of supernatant is shown in Fig. 5. The presence of strong acyclic C–H stretching at 2924 and 2855 cm^{-1} demonstrates the coexistence of free oleic acid and oleylamine. The discernible peak at 1412 cm^{-1} is assigned to the carboxylate (COO^-) stretch, while the obvious peaks at 1560 and 1647 cm^{-1} are attributed to the C–N stretch of amide. Other peaks at 1051, 1083 and 3431 cm^{-1} could be ascribed to vibrations of bonds in ethanol. These FT-IR data confirm that OAm and OAc make amidation reaction and produce H_2O, which is consistent with the experimental phenomenon that some low-boiling substances condenses on the upper part of the flask during synthesis reaction. This indicated that when we added the S-OAm solution into the three-necked flask, oleylamine molecules, which had been

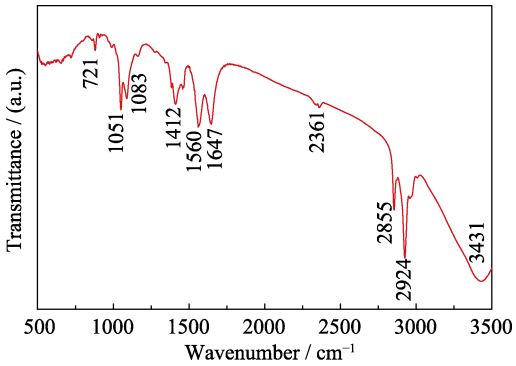

Fig. 5 FT-IR spectrum of reaction solution

combined with S, was rapidly amidated with the original oleic acid to form water and rapidly released reactive S.

The 2D nano plate morphology arises from the anisotropic bonding nature of SnS_2, since the intra-layer covalent bond is stronger than the interlayer van der Waals force. Due to the large amount dangling bonds exist on the edge of the growing nucleation, the growth of SnS_2 crystals continues with a high anisotropic nature, and Sn and S atoms would selectively bind to these dangling bond sites. Thus, the lateral dimension grows much faster than the vertical thickness dimension, which results in the thin plate morphology of SnS_2.

In the typical synthetic method, the molar ratio between oleylamine and oleic acid was about 1 : 1, which resulted in a moderate S generation rate and nucleation rate, and subsequently further reaction prepared typical SnS_2 NPs with uniform hexagonal shape.

We also investigated the effect of surfactants on the morphology of SnS_2 NPs. Fig. 6 shows TEM images of SnS_2 NPs with different molar ratio between OAc and OAm. From Fig. 6(a) to 6(i), the amount of OAm decreases, while that of OAc increases. As shown in Fig. 6(a), with

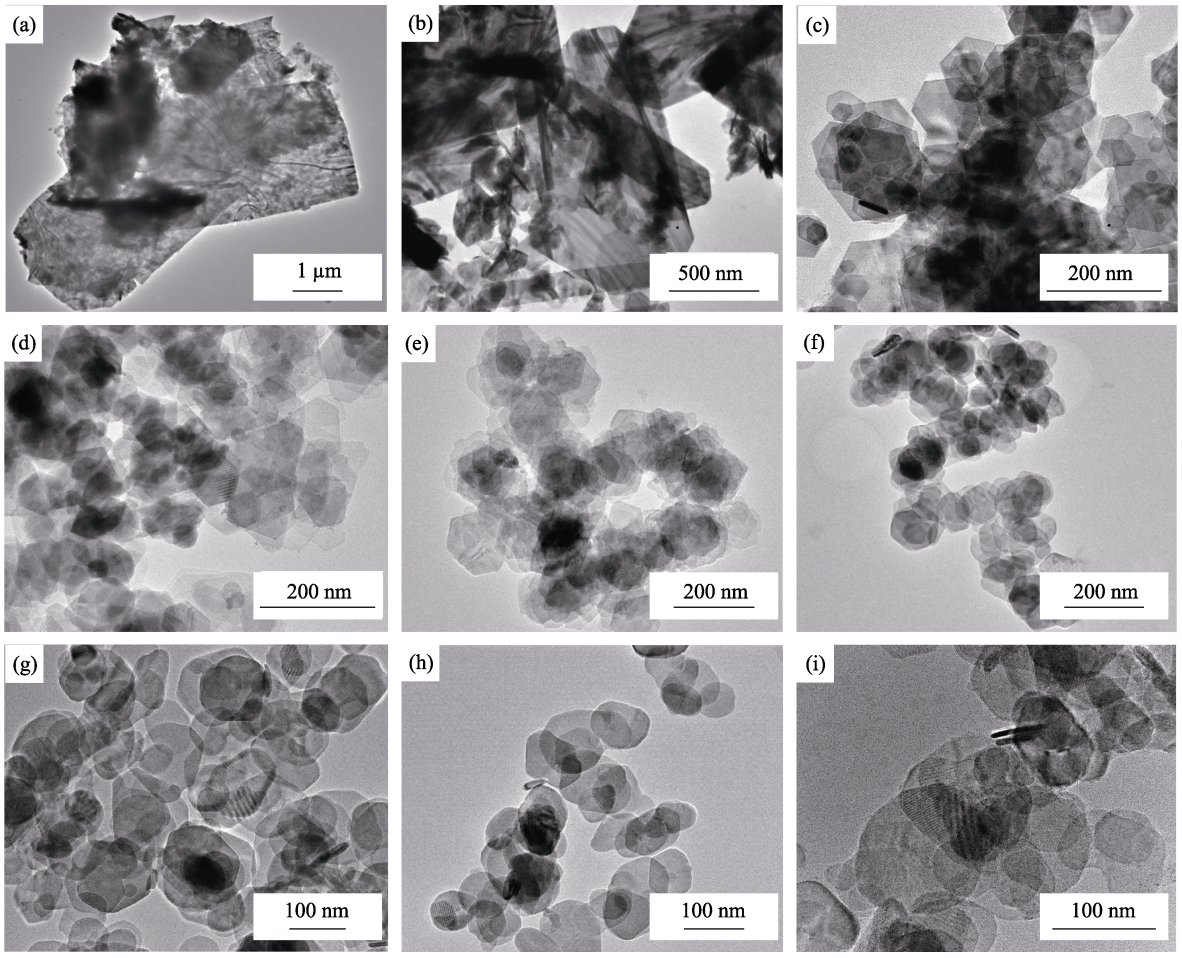

Fig. 6　TEM images of SnS_2 NPs with different molar ratio of OAc to OAm from 1∶9 to 9∶1 (a-i)

little oleic acid participating in the reaction, the morphology of product is quite different from the typical one. Its lateral size is up to 10 μm. When the mixed solution containing S and oil amine was injected into the flask, some of them made amidation reaction with OAc as above and generated SnS_2 nucleus, while the remaining S-OAm solution released H_2S[24]. The latter process is much slower than the former, resulting in a low nucleation rate and less number of nucleation. During the whole reaction process, more S and Sn participate in the growth of the NPs; and some of oleylamine molecules tend to interact with S atom exposed on the outer (001) crystal face of SnS_2 NPs so that the laterial size of this sample is great. As shown in Fig. 6(i), when oleic acid is excessive, almost all OAm moleculars instantaneous amide with OAc moleculars and release a lot of S precursors, which produce much more nucles than those of typical synthesis. In addition, excessive OAc moleculars bonded to Sn atoms exposed on the edge of SnS_2 NPs, and this interaction hinders growing along the lateral dimension. Therefore the morphology of this sample is circle instead of hexagon, and its lateral size is small. The whole reaction and growth process is shown in Fig. 7.

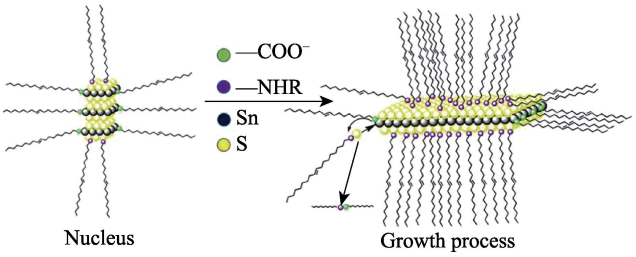

Fig. 7　Growth process of SnS_2 NPs

2.4　Gas sensing properties

A large number of studies has demonstrated that the operating temperature of a gas sensor is the most influential factor which affects the gas response of semiconductor sensors[25]. It is known that sulfides are unstable in the air at high temperatures, so we examined the stability of the as-prepared SnS_2 NPs. After heating the NPs to 150 ℃ in air for 8 d, XRD result showed that there was no transition from SnS_2 to SnO_x. And our previous research also shows that SnS_2 phase tends to fade for the sample treated at 250 ℃[26]. Therefore, we tested the gas sensing response of SnS_2 NPs at operating temperatures from room temperature to 150 ℃. At room

temperature (20 ℃), there is no acceptable signal because the resistance of the sensing device is too large for the test limit of the ammeter. The response curves of sensors made of typical SnS_2 NPs in the presence of 10^{-5} of NO_2 gas at 50–150 ℃ are shown in Fig. 8. The current in the test circuit in the air increased with the growing of temperature. This is because more electron-absorbing thermal energy transitions from the valence band to the conduction band, causing the resistance of the material to decrease. SnS_2 is an n-type semiconductor and NO_2 molecule is an electron acceptor. When we injected NO_2 gas into the test chamber, NO_2 molecules were adsorbed on the surface of SnS_2 NPs, and electrons in the conduction band of SnS_2 NPs transferred to NO_2 molecules, causing the number of conduction band electrons reducing, which made the resistance of SnS_2 NPs increase[27]. When the temperature below 90 ℃, there were less conduction band electrons. So in NO_2 atmosphere, almost all electrons were transferred to NO_2 molecules, leading to the fact that resistance was extremely large and the current value was close to 0. At this time, S is infinite and the response of SnS_2 NPs to NO_2 gas is obvious. At the same time, however, the gas desorption rate at low temperatures was very slow, and it was clear that when the test device was placed back in the air, the resistance could not return to the pre-adsorption level in an acceptable time range. When the operating temperature reached 130 ℃, the sensing time (t_{sen}) and recover time (t_{rec}) was 98 s and 680 s, respectively, and S was 4.14. Then, when the temperature continued to rise to 150 ℃, t_{sen} increased to 168 s and S also decreased to 3.13. So 130 ℃ is the optimum temperature for the detection of NO_2 gas by SnS_2 NPs prepared in this study.

Fig. 9(a) shows the dynamic sensing-recovery curves of the sensors to NO_2 gas with concentrations ranging from 20×10^{-6} to 0.5×10^{-6} at 130 ℃. With the decrease of NO_2 concentration, S was getting weaker and weaker. This is due to less ethanol molecules adsorbed on the surface of the sensing material, and the resistance of SnS_2 NPs with less change. When the concentration of NO_2 gas decreased to 0.5×10^{-6}, the gas sensor still performed an obvious response, revealing the resistance of the prepared SnS_2 NPs is very sensitive to NO_2 gas. Furthermore, we believe that the lowest detection concentration should be less than 10^{-7}, but due to limitations of experimental conditions, we can't accurately measure the response signal at lower concentrations.

In order to study their reversibility characteristics, sensing devices were exposed to 10^{-5} of NO_2 gas and air alternately for 3 or more cycles. In Fig. 9(b), we can see the resistance of sensor in 10^{-5} NO_2 gas was steady and can return to no-load level after each desorption. This result confirms that there is a minuscule amount of gas molecules during desorption process, and this SnS_2 NPs gas sensors have a good performance in reversible cycle tests. We also tested the responses of this SnS_2 NPs

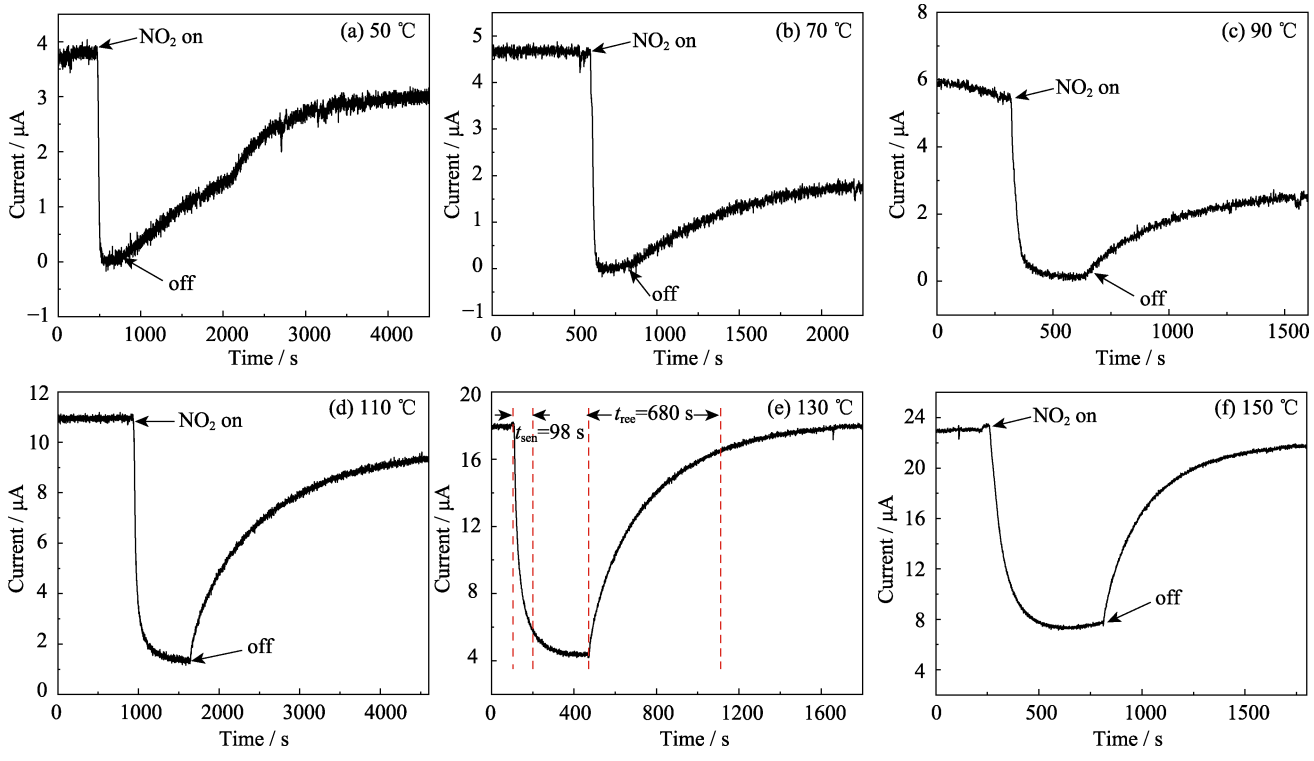

Fig. 8 Response curves of sensors made of typical SnS_2 NPs in the presence of 1×10^{-5} of NO_2 gas at different operating temperatures

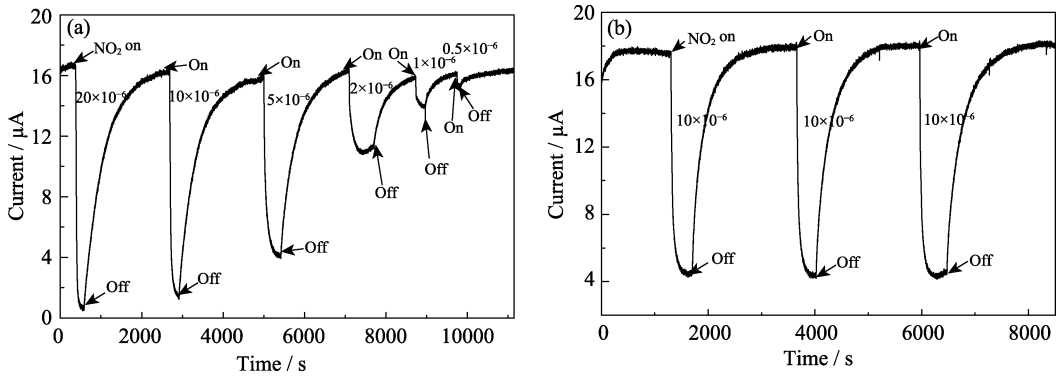

Fig. 9 (a) Dynamic sensing performance of SnS_2 NPs toward NO_2 gas at concentrations ranging from 20×10^{-6} to 0.5×10^{-6} at 130 ℃, and (b) three reversible test cycles of SnS_2 NPs toward 10×10^{-6} NO_2 at 130 ℃

based sensors to different gases at 130 ℃. Experiments have shown that SnS_2 NPs was not sensitive to ammonia (100×10^{-6}), carbon dioxide (3%) and hydrogen (20×10^{-6}). This indicates the SnS_2 NPs based sensors exhibit superior selectivity to NO_2 gas.

3 Conclusions

Uniform hexagonal shape SnS_2 NPs with a thickness of 4–6 nm and lateral dimensions of about 150 nm were obtained by high temperature chemical bath method. The ratio between OAm and OAc is the key to control the morphology of SnS_2 NPs. During the process of nucleus growth, OAm will attach to exposed (0001) crystal surface and prevent NPs vertical growth. To add amount of OAm, we got a series of SnS_2 nanoplates with huge lateral size. The gas sensing properties of 2D SnS_2 NPs were investigated at different operating temperatures. 2D SnS_2 NPs based sensors exhibited excellent sensing properties to NO_2 gas with a response *S* of 4.14 at 130 ℃, a sensing time of 98 s and a recovery time of 680 s. This study demonstrates the potential of 2D SnS_2 NPs for NO_2 gas sensing applications.

References:

[1] WANG Z, YUAN X X, CONG S, *et al*. Color-changing microfiber-based multifunctional window screen for capture and visualized monitoring of NH_3. *ACS Applied Materals and Interfaces*, 2018, **10:** 15065–15072.

[2] SONG X F, HU J L, ZENG H B, *et al*. Two-dimensional: recent progress and future perspectives. *Journal of Materials Chemistry C*, 2013, **1:** 2952–2969.

[3] SABOOR F H, KHODADADI A A, MORTAZAVI Y, *et al*. Microemulsion synthesized Silica/ZnO stable core/shell sensors highly selective to ethanol with minimum sensitivity to humidity. *Sensors and Actuators B*, 2017, **238:** 1070–1083.

[4] LI X L, LOU T J, SUN X M, *et al*. Highly sensitive WO_3 hollow-sphere gas sensors. *Inorganic Chemistry*, 2004, **43(17):** 5442–5449.

[5] LI S M, ZHANG L X, ZHU M Y, *et al*. Acetone sensing of ZnO nanosheets synthesized using room-temperature precipitation. *Sensors and Actuators B*, 2017, **249**: 611–623.

[6] LEE J H, KATOCH A, CHOI S W, *et al*. Extraordinary improvement of gas-sensing performances in SnO_2 nanofibers due to creation of local p-n heterojunctions by loading reduced graphene oxide nanosheets. *ACS Applied Materials & Interfaces*, 2015, **7(5):** 3101–3109.

[7] BARUWATI B, KUMAR D K, MANORAMA S V. Hydrothermal synthesis of highly crystalline ZnO nanoparticles: a competitive sensor for LPG and EtOH. *Sensors and Actuators B*, 2006, **119:** 676–682.

[8] BAGHERI M, HAMEDANIA N F, MAHJOUBA A R, *et al*. Highly sensitive and selective ethanol sensor based on Sm_2O_3-loaded flower-like ZnO nanostructure. *Sensors and Actuators B*, 2014, **191:** 283–290.

[9] SONG P, HAN D, ZHANG H H, *et al*. Hydrothermal synthesis of porous In_2O_3 nanospheres with superior ethanol sensing properties. *Sensors and Actuators B*, 2014, **196:** 434–439.

[10] SEO J W, JUN Y, PARK S W, *et al*. Two-dimensional nanosheet crystals. *Angewandte Chemie-international Edition*, 2007, **46(46):** 8828–8831.

[11] NOVOSELOV K S, JIANG D, SCHEDIN F, *et al*. Two-dimensional atomic crystals. *Proceedings of the National Acadamy of Sciences of the United States of America*, 2005, **102(30):** 10451−10453.

[12] SEO J W, JANG J T, PARK S W, *et al*. Two-dimensional SnS_2 nanoplates with extraordinary high discharge capacity for lithium ion batteries. *Advanced Materials*, 2008, **20(22):** 4269–4273.

[13] KIM Y H, PHAN D T, AHN S, *et al*. Two-dimensional SnS_2 materials as high-performance NO_2 sensors with fast response and high sensitivity. *Sensors and Actuators B*, 2018, **255:** 616–621.

[14] PERKINS F K, FRIEDMAN A L, COBAS E, *et al*. Chemical vapor sensing with monolayer MoS_2. *Nano Letters*, 2013, **13(2):** 668–673.

[15] LI H, YIN Z, HE Q, *et al*. Fabrication of single and multilayer MoS_2 film based field effect transistors for sensing NO at room temperature. *Small*, 2012, **8:** 63–67.

[16] SHI W, HUO L, WANG H, *et al*. Hydrothermal growth and gas sensing property of flower-shaped SnS_2 nanostructures. *Nanotechnology*, **17(12):** 2918–2294.

[17] HUANG Y, SUTTER E, SADOWSKI J T, *et al*. Tin disulfide—an emerging layered metal dichalcogenide semiconductor: materials properties and device characteristics. *ACS Nano*, 2014, **8(10):** 10743–10755.

[18] SU G X, HADJIEV V G, LOYA P E, *et al*. Chemical vapor deposition of thin crystals of layered semiconductor SnS_2 for fast photodetection application. *Nano Letters*, 2015, **15(1):** 506–513.

[19] ZHAI C X, DU N, ZHANG H, *et al*. Large-scale synthesis of ultrathin hexagonal tin disulfide nanosheets with highly reversible lithium storage. *Chemistry Communications*, 2011, **47(4):** 1270–1272.
[20] MA J M, LEI D N, DUAN X C, *et al*. Designable fabrication of flower-like SnS_2 aggregates with excellent performance in lithium-ion batteries. *RSC Advances*, 2012, **2(9):** 3615–3617.
[21] KUMAR G M, XIAO F, ILANCHEZHIYAN P, *et al*. Enhanced photoelectrical performance of chemically processed SnS_2 nanoplates. *RSC Advances*, 2016, **6(102):** 99631–99637.
[22] TAN C L, CAO X H, WU X J, *et al*. Recent advances in ultrathin two-dimensional nanomaterials. *Chemical Reviews*, 2017, **117(9):** 6225–6331.
[23] DU Y P, YIN Z Y, RUI X H, *et al*. A facile, relative green, and inexpensive synthetic approach toward large-scale production of SnS_2 nanoplates for high-performance lithium-ion batteries. *Nanoscale*, 2013, **5(4):** 1456–1459.
[24] THOMSON J W, NAGASHIMA K, MACDONALD P M, *et al*. From sulfur−amine solutions to metal sulfide nanocrystals: peering into the oleylamine−sulfur black box. *Journal of the American Chemicak Society*, 2011, **133(13):** 5036−5041.
[25] SHI J J, CHENG Z X, GAO L P, *et al.* Facile synthesis of reduced graphene oxide/hexagonal WO_3 nanosheets composites with enhanced H_2S sensing properties. *Sensors and Actuators B*, 2016, **230:** 736–745.
[26] LI Y X, LEONARDI S G, BONAVITA A, *et al*. Two-dimensional (2D) SnS_2-based oxygen sensor. *Procedia Engineering*, 2016, **168:** 1102–1105.
[27] OU J Z, GE W Y, CAREY B, *et al*. Physisorption-based charge transfer in two-dimensional SnS_2 for selective and reversible NO_2 gas sensing. *ACS Nano*, 2015, **9(10):** 10313-10323.

SnS_2 纳米片的制备及其对 NO_2 气体的检测

山 巍[1,2], 傅正钱[1], 张发强[1], 马名生[1], 刘志甫[1,2], 李永祥[1,2]

(1. 中国科学院 上海硅酸盐研究所, 上海 200050; 2. 中国科学院大学 材料与光电研究中心, 北京 100049)

摘 要: 二维金属硫化物材料具有较低的电子噪声以及极大的比表面积, 使其非常适合用作气敏材料, 因此寻求高效可控的方法制备二维金属硫化物材料是目前的研究热点。本研究使用高温化学浴法制备了不同形貌的高结晶二维六方 SnS_2 纳米片。采用不同手段对制备的 SnS_2 纳米片进行表征, 并进一步研究了 SnS_2 纳米片的气敏性能。结果显示: 油酸、油胺用量(体积)相同时, 产物 SnS_2 的形貌是均一的六角形纳米片, 其直径约 150 nm, 厚度约 4~6 nm。气敏测试表明该 SnS_2 纳米片对 NO_2 气体具有良好响应, 且响应过程可逆, 选择性好。其最佳工作温度为 130 ℃, 响应和恢复时间分别为 98 和 680 s。

关 键 词: 二氧化氮气体; 二维材料; SnS_2; 高温化学浴法; 气敏检测

中图分类号: TQ174 **文献标识码:** A